Fluid substitution in coalbeds

Diane J. Lespinasse and Robert J. Ferguson

ABSTRACT

We present an evaluation of the seismic response due to fluids in the pore space of coalbeds. The objective of this project is to perform a fluid substitution in coalbeds and generate the associated synthetic seismograms by implementing a work flow previously developed to evaluate seismic as a monitoring tool for CO_2 sequestration in coals.

The Mannville coals are one of the most important coalbed methane resources in the Alberta Province, Western of Canada. In order to study the Mannville Group coals we selected the Corbett Field, located 145Km to the NW of Edmonton, as the area of study. In the Corbett Field the targets are two coal seams of the Mannville Group, the Main Seam with 4m thickness and the Lower Seam, with a thickness of 1.5m.

Using well log data from the well 100-03-22-062-06W500 of the Corbett Field, we perform a fluid simulation to make an assessment of its production forecast in a 10 years period and complete a fluid substitution. We use Gassmann equation to substitute 100% brine (initial state) in the pore space of Main Seam and Lower Seam by a combination of brine and methane.

We also present synthetic seismograms for coalbeds of 10m and 21m thickness in order to establish seismic resolution limits.

INTRODUCTION

Coalbed methane caught the attention of the world due to its potential to become an important source of natural gas (Shi and Durucan, 2005). As a consequence, studies that aim to determine the physical properties of coals, enhance the production of coalbed methane and improve the characterization of coal reservoirs are increasingly important. Clarkson and Bustin (2010) present a review of the techniques available for coal reservoir characterization and summarize the challenges that can be found in coalbed methane production; McCrank and Lawton (2009), use seismic to monitor a CO_2 flood injected in the Ardley coals, and Zarantonello et al. (2010) developed a work flow to generate a seismic model associated with the storage of CO2 in coalbeds.

In this project we show the variation in the seismic response that occurs due to the substitution of brine by brine and methane in coalbeds from the Corbett Field. In this area, we select to coal seams, Main seam (4m) and the Lower seam (1.5m), of the upper part of the Mannville Group.

Initially, we present a fluid simulation to predict the reservoir production history, the proportions of brine and methane in the pore space during production, and the variations of the reservoir pressure and the coal matrix changes during depletion. With this information, we complete a fluid substitution in the Main Seam and Lower Seam

assuming an initial state of 100% brine in the pore space and a final state of 82% of brine and 18% of methane (after 8 years of production) and generate the synthetic seismograms.

Coalbed Methane (CBM)

Coalbed Methane (CBM) is catalogued as an unconventional resource in which the coalbed acts as a source and as a reservoir rock (McCrank and Lawton, 2009). An important characteristic of coalbeds is that they have two porosity systems (Deisman et al., 2009). There is a microporosity system which controls the gas accumulation into the coal and the macroporosity system that is thought as the one that determines the coalbeds permeability (Clarkson and Bustin, 2010).

Methane can be found in coalbeds as a free gas in the porous space or adsorbed in its structure. The CBM present in the pore space, as a free gas, represents the 10% of the CBM and is normally in company of gases like N_2 and CO_2. The other 90% of the CBM is adsorbed into its matrix due to the effect of the Van der Waal forces (Peng et al., 2006).

The production of the CBM takes place when a reduction of the pressure at a reservoir level causes desorption of the methane from the matrix (FIG. 1). In this way, the gas starts to flow through the porosity system until it reaches the wellbore. In presence of coalbeds with high water content, the process begins with water production that will bring as a consequence the pressure reduction required for the methane desorption (Clarkson and Bustin, 2010).

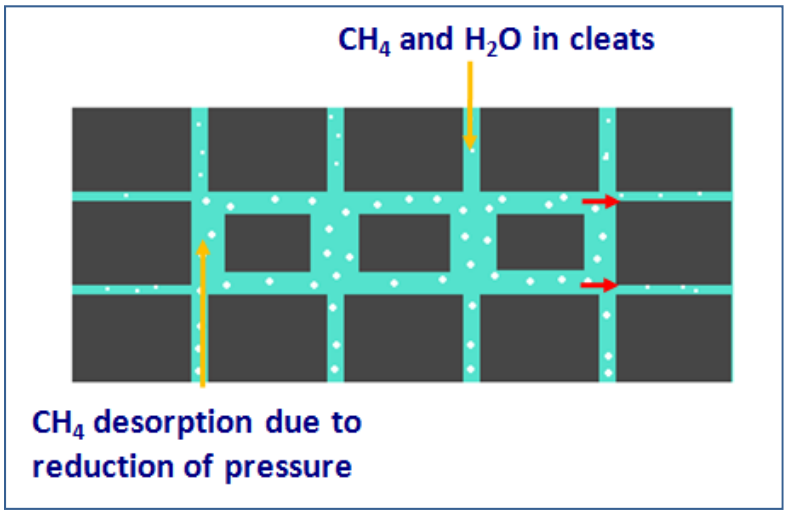

FIG. 1. Methane desorption from coal matrix. As reservoir pressure decrease as consequence of water production, methane desorps from the coal matrix

Factors like gas saturation and composition as well as changes in reservoir pressure are important during CBM production process because they can affect the porosity systems in coals and can also have an important impact in the stability of the wellbore (Deisman et al., 2009). It is also important to consider that the methane desorption causes

shrinkage of the coal matrix generating permeability increase. As the coal matrix shrinks, there is an increase of the cleat spacing (FIG. 2) (Palmer and Mansoori, 1998).

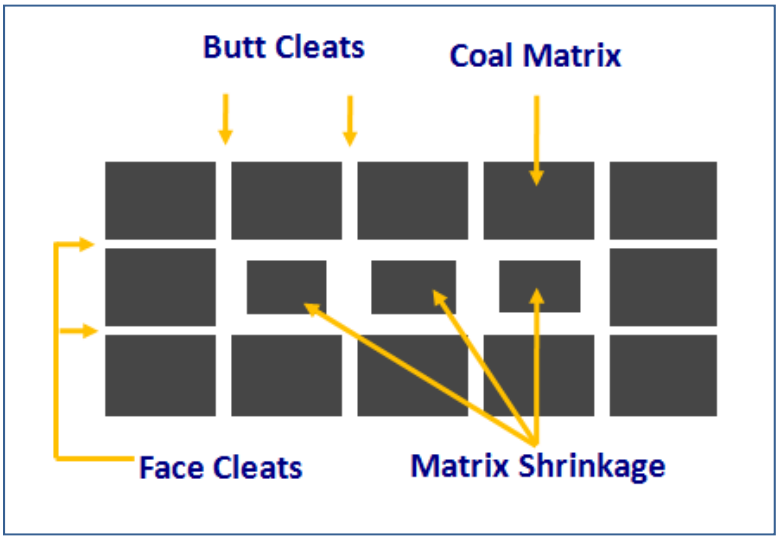

FIG. 2. Coal matrix shrinkage due to methane desorption

Enhance Coalbed Methane (ECBM)

Enhanced Coalbed Methane (ECBM) is a technique that causes the methane desorption by fluid injection into the coalbed (McCrank and Lawton, 2009). The process involves the adsorption of the injected gas, replacing the methane and as a consequence improving the production rates (Robertson, 2008). An important aspect that should be considered, during the application of this technique, is that due to the interaction of the injected fluid with the coal, the coal matrix properties can suffer alterations or changes (Balan and Gumrah, 2008)

N_2 and CO_2 represent two options for the ECBM . In the case of the N_2, the injection generates a variation in the pressure producing a release of methane from the coal (McCrank and Lawton, 2009). The displacement of methane by N_2 occurs in order to compensate the pressure variation and to restore the balance into the coal. In addition, when the N_2 reaches the coal, an increment of the permeability occurs, leading to an increase of the injectability rate and to an early leakage of N_2 (Koperna and Oudinot, 2009)

The ECBM using CO_2 brings an extra benefit in which coals can act as sites for CO_2 sequestration in the subsurface contributing in the reduction of the emissions of gases that cause the greenhouse effect (Koperna and Riestenberg, 2009). Studies have determined that coal has more predisposition to adsorb CO_2 than CH_4 and N_2 (FIG.3), being able to store big quantities of CO_2 (Koperna and Oudinot, 2009).

During CO_2-ECBM, there are two processes that produce an alteration of the coal structure; these processes are: adsorption and dissolution of CO_2 (Karacan, 2007). In general, after injection, the CO_2 is adsorbed by the coal releasing methane, which moves

through the most permeable areas for production (Koperna and Oudinot, 2009). The dissolution of the CO_2 and its interaction with the coal has a swelling effect in the coal matrix (Karacan, 2007) generating changes in the permeability, limiting the movement of the gases through the coalbed and decreasing the CO_2 injection rate (Chen et al., 2009). This swelling effect is more evident in the area adjacent to the wellbore (Karacan, 2007

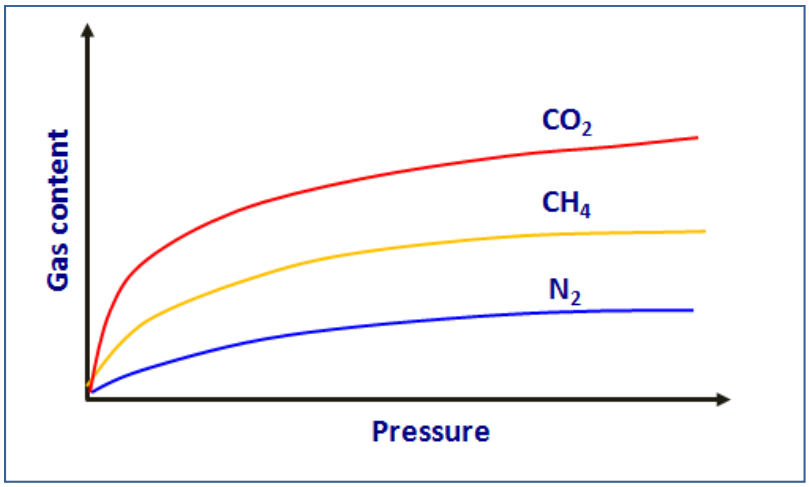

FIG. 3. Examples of adsorption isotherms of coals. This graph presents the preferential adsorption of CO_2 in coals.

The swelling of the matrix is an important factor to consider because it can provide information about the rate at which the CO_2 is absorbed by the coal, volume changes in the coal and the variations that occur in terms of the permeability (Karacan, 2007). The swelling process in coalbeds can bring some complications in the development of ECBM and CO_2 storage projects (Chen et al., 2009).

THEORETICAL DEVELOPMENT

Coal permeability modelling

Langmuir Isotherm

In coalbeds, methane is present in the cleats and is also adsorbed in the coal matrix (Peng et al., 2006). The methane adsorption and desorption in coalbeds can be modeled with the Langmuir isotherm equation (Shi and Durucan, 2005) which allow the estimation of the gas content in terms of pressure. Equation 1 represents the Langmuir isotherm:

$$V = V_L \frac{P}{P_L + P}, \quad (1)$$

where V is the adsorbed volume of methane, V_L is the Langmuir Volume or the maximum volume of adsorbed methane when pressure tends to infinite, P_L is the pressure

at which the adsorbed methane volume V becomes half of the Langmuir Volume $V_L/2$ and P is the pressure (Robertson, 2008).

This relationship establishes that the permeability of the cleats does not change linearly with the reduction of the pressure (Shi and Durucan, 2005) and assumes a homogeneous media in which the adsorbed molecules do not interact between each other and the surrounded media (Bell and Rakop, 1986)

Palmer and Mansoori model

During production in coalbed reservoirs, two factors influence the changes in permeability. The first one is the compression of the cleats due to an increasing of the effective stress that leads to a reduction of the permeability. The second one is the matrix shrinkage generated by the methane desorption as consequence of the decreasing of the reservoir pressure; causing an increasing of the permeability (Palmer and Mansoori, 1998). In 1998, Palmer and Mansoori developed a permeability model for coal reservoirs.

Palmer and Mansoori permeability model (Palmer and Mansoori, 1998) calculates the variations in permeability as a consequence of the pressure decrease during reservoir depletion and the shrinkage of the matrix caused by methane desorption (Palmer, 2009). The Palmer and Mansoori model (Palmer and Mansoori, 1998) is defined by the following equation:

$$\frac{\phi}{\phi_i} = 1 + \frac{C_f}{\phi_i}(P - P_i) + \frac{\varepsilon_\infty}{\phi_i}\left(\frac{K}{M} - 1\right)\left(\frac{P}{P+P_\varepsilon} - \frac{P_i}{P_i+P_\varepsilon}\right), \quad (2)$$

and,

$$C_f = \frac{1}{M} - \left(\frac{K}{M} + f - 1\right)\beta, \quad (3)$$

where ϕ is the cleat porosity, ϕ_i is the cleat porosity at the initial reservoir pressure, $\frac{C_f}{\phi_i}$ is the fracture compressibility, P is pressure, P_i is the initial reservoir pressure, ε_∞ is the volumetric strain at infinite pressure, P_ε is the pressure at a strain equals to $0.5\varepsilon_\infty$ or Langmuir Pressure, K is the Bulk Modulus, M is the constrained axial modulus, β is the grain compressibility and f is the fraction (Clarkson et al., 2010). In the Palmer and Mansoori model (Palmer and Mansoori, 1998), porosity and permeability are related by equation 4.

$$\frac{k}{k_i} = \frac{\phi^3}{\phi_i^3}, \quad (4)$$

where k is the permeability and k_i is the initial permeability (Palmer and Mansoori, 1998).

Fluid substitution and Gassmann equation

The fluid substitution is a technique that estimated changes in the seismic response as well as in density that occur as a consequence of variations in the fluid saturations in a reservoir (Kumar, 2006). This technique allow us to evaluate the response that we should obtain for an specific fluid or mix of fluids in the pore space, based on the real conditions of the reservoir at the moment in which the well data was measured (Dvorkin et al., 2007).

The fluid substitution is an important method that provides complementary information for well data analysis (Dvorkin et al., 2007), evaluation of amplitude versus offset response and development of 4D surveys (Smith et al., 2003). More than that, this tool makes possible the estimation of seismic velocities and density during the different stages of a reservoir, based on the fluid saturations (Han and Batzle, 2004).

Gassmann (1951) developed and equation for fluid substitution that relates the bulk modulus of the saturated rock with the porous space, pore fluid properties, mineral composition and the frame of the rock (Dvorkin et al., 2007). Equation 5 represents a general form of Gassmann's equation (Gassmann, 1951).

$$K_{sat} = K^* + \frac{\left(1-\frac{K^*}{K_0}\right)^2}{\frac{\phi}{K_{fl}}+\frac{(1-\phi)}{K_0}-\frac{K^*}{K_0^2}} \quad , \tag{5}$$

where K_{sat} is the bulk modulus of the saturated rock, K^* is the bulk modulus of the dry rock, K_0 is the bulk modulus of the mineral matrix, $K_{fl}$is the bulk modulus of the fluid in the pore space and ϕ is the porosity (Smith et al., 2003).

During the formulation of Gassmann's equation (Gassmann, 1951), some assumptions were done. In first place, Gassmann's equation (Gassmann, 1951) assumes an isotropic media that presents a homogeneous and monomineralic matrix. This assumption is usually violated because the majority of the rocks present a certain degree of anisotropy (Han and Batzle, 2004). Secondly, this equation assumes that the pores are connected allowing the movements of the fluids through them (Smith et al., 2003). Finally, between the pore fluids and the frame of the rock, there are not chemical interactions that can modify the frame properties of the rocks along the time (Han and Batzle, 2004). This last assumption lead to an important condition, the bulk modulus of the rock frame and the shear modulus will remain as constants during the fluid substitution process (Smith et al., 2003).

In practice, to do a fluid substitution is necessary to calculate the in-situ conditions, to obtain the bulk modulus of the frame of the rock. The in-situ conditions are obtained from well log information, allowing the calculation of K_{sat} and K_{fl} for the initial conditions as well as the shear modulus (Kumar, 2006). Using equation 5, now it is possible to determine the bulk modulus of the dry rock (frame of the rock). After the properties of the dry rock are estimated, it is possible to calculate (using the same equation) properties of the rock saturated with a new fluid (Smith et al., 2003).

AREA OF STUDY

The area of study is the Corbett Field in the Corbett Creek area, 145Km to the NW of Edmonton (Cockbill, 2008). The Corbett Field has an extension of approximately 558 Km^2 and is located in the north central part of Alberta, Canada. This area was selected in order to study the Mannville Formation coals, which contain 64% of the reserves of natural gas that comes from coals in Alberta (Gentiz et al., 2008). A map showing the location of the area of study is presented in FIG. 4.

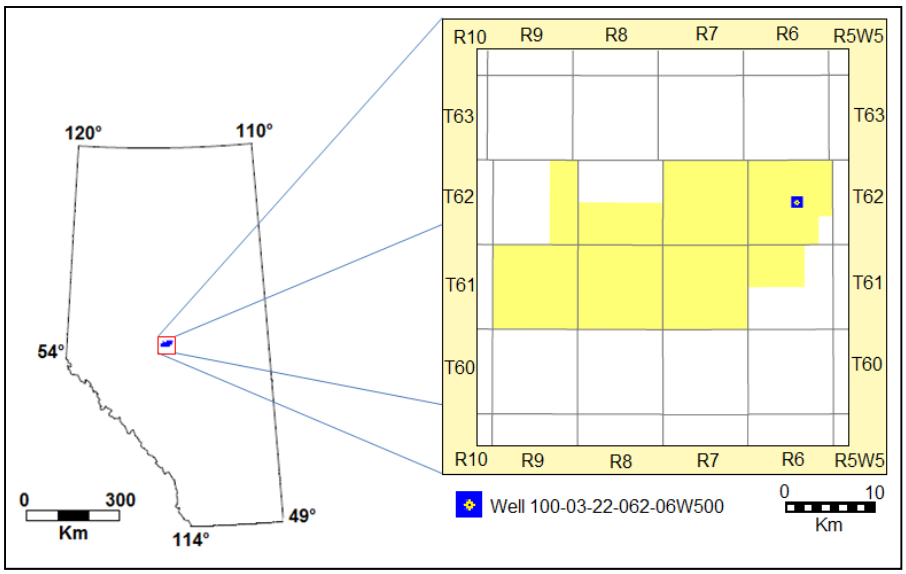

FIG. 4. Corbett Field and 100-03-22-062-06W500 well location.

The first well in Corbett Field was drilled during 2000, reaching two coal seams of the Upper part of the Mannville Group. Production activity started in January 2002 and those coal seams became the target. The coal seams are at a depth of approximately 825m in the NE area of the field, and become deeper to the SW where they reach a depth of approximately 1080m (Cockbill, 2008). The first seam is known as the Main Seam and it has a thickness of approximately 4m while the second one, or Lower Seam, is thinner and presents an average thickness of 1.5-2m. Overlying and underlying the Main and Lower seam, there are several coal seams, but they are thinner and have limited lateral extension (Gentiz et al., 2008).

Vertical wells were drilled in the Corbett Field which result in gas production of 20mcf/d-100 mcf/d. In 2004, horizontal wells were drilled in order to decrease the dewatering time and increase the gas production. The horizontal wells increase the production to 200mcf/d-700mcf/d. Since 2005 to the present moment, multi-lateral horizontal wells has been drilled which produce an average of 2mmcf/d of gas (Cockbill, 2008).

Well log data from the well 100-03-22-062-06W500 was used for the development of this project. FIG. 4 shows the location of the well and FIG. 5 presents the well log data.

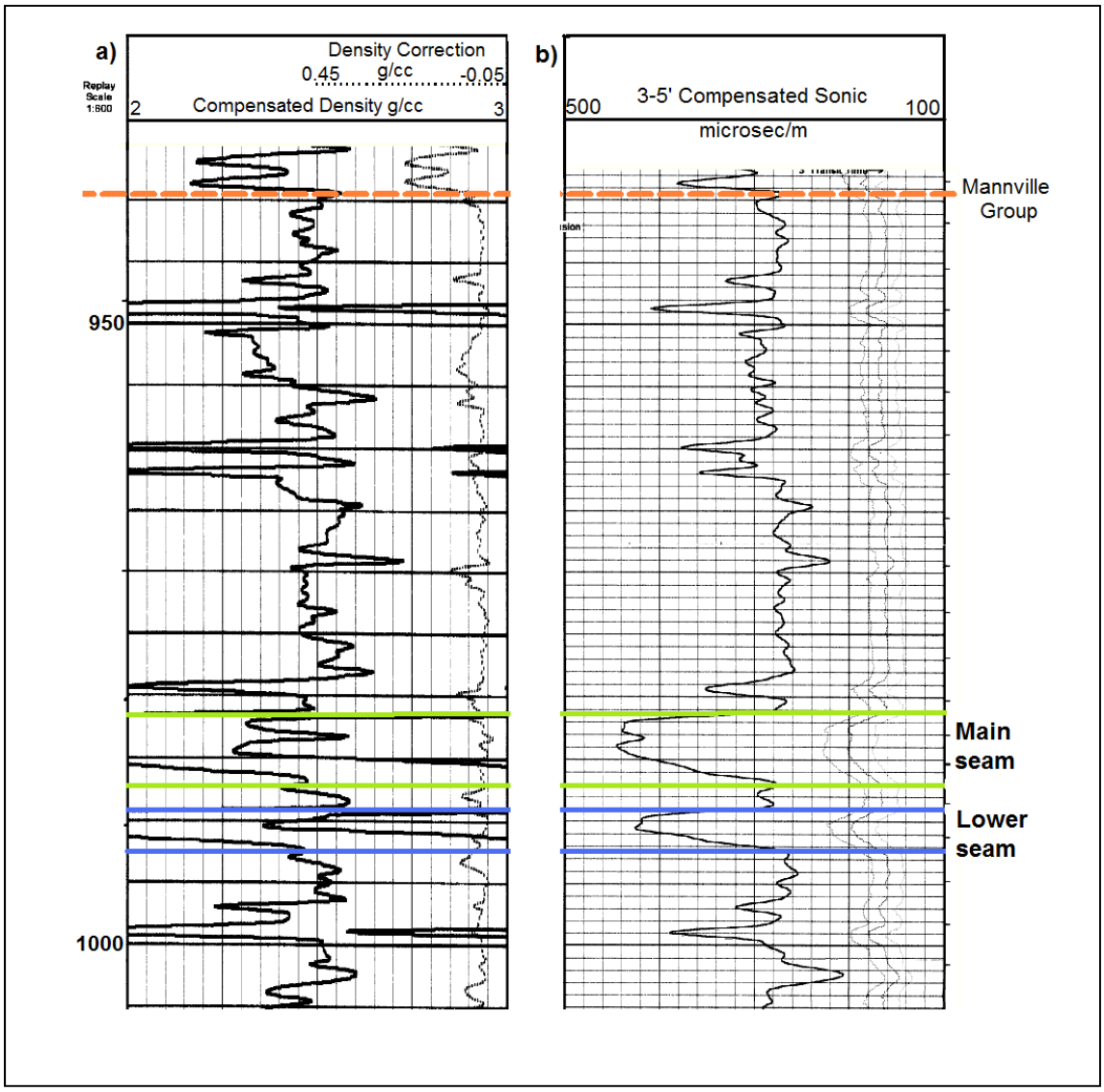

FIG. 5. Well log of the well 100-03-22-062-06W500. a) Compensated density log and b) Compensated sonic log.

Mannville Group

Mannville Group, Ardley Coals (including Coalspur Coal, Ardley Coal equivalent in the Foothills), Horseshoe Canyon Formation and Belly River Group represent the four major coal areas in Alberta, being the Mannville Group coals the ones with the highest gas content (Beaton, 2003).

The deposition of the Mannville Group took place during the Lower Cretaceous and extends through the southern and central Alberta Plains (Beaton, 2003). The Mannville Group is underlying the Colorado Group and overlying the pre-Cretaceous unconformity (Gentiz et al., 2008).

The base of the Mannville Group consist of sediments deposited in continental (alluvial and fluvial) and transitional (deltaic and estuarine) environments, which filled the paleotopography generated by the erosion period (Beaton et al.,2006). The Lower Mannville deposition ends with a regional transgression of the sea. (Beaton, 2003).

A progradational sequence defines the middle Mannville (Banerjee and Goodarzi, 1990), with sediments from shoreline till fluvial and estuarine environments (Beaton, 2003). Finally, Upper Mannville is characterized by cycles of regressive and transgressive sequences in which several coal seams were deposited (Beaton et al.,2006).

The deposition of the coals from the Upper part of the Manville Group occurred in a fluvio-deltaic environment, and they have their origin in wood and plants that suffered a coalification process(Gentiz et al., 2008).These coal seams are known for being deep (475m in the NE to 3600m in the SW) (Bachu, 2007), thick and with a low percentage of ash content (Gentiz et al., 2008).

Upper Mannville coal rank is sub-bituminous to high volatile bituminous and it has a net thickness that varies from 0.2 to 16.5m, reaching the maximum thickness in the west and central part of Alberta (Bachu, 2007). Red Dear represents one of the areas with the thickest net coal (6-12m) in the Upper part of the Mannville Group while the average net thickness is in the range of 2-6m (Beaton et al., 2006).

In general, Mannville coals zones present temperatures higher than 31°C and formation water with high salinity (Bachu, 2007). Additionally, the gas estimation is in the order of 5bcf/section for the areas that present a net coal thickness of approximately 4m (Beaton et al.,2006).

Corbett Creek coal properties

The reflectance of the vitrinite in this area was determined by core tests and it is in the range of 0.62%-0.67%. Core tests also determined the existence of bright as well as bright-dull (banded) lithotypes. In addition, the presence of Siderite was identified in cleats (Gentiz et al., 2008).

The three major maceral groups are identified in Corbett Creek coals. Vitrinite is in the form of massive collotelinite while Liptinite can be found in different forms including resinite, sporonite and exudanite. The third group, Inertinite, is mostly represented by the presence of telo-inertinite (Gentiz et al., 2008). .

The estimated porosity for Mannville Coals in this area is 5-6% and they have a permeability of 3-4mD. As a result of the representative presence of vitrinite in Corbett Creek coals, there was a good formation of the cleat system, showing face cleats at an interval of 0.5 cm. The gas content has been estimated in 6-8 cm^3/g and the gas composition in these coals is mostly methane (94%) and small proportions of CO_2, N_2 and ethane (Gentiz et al., 2008).

METHODOLOGY

Data set selection and data collection

For the development of this project, well log data from HorseShoe Canyon (Bashaw Field) and Manville Coals (Corbett Field) were available. The two data sets were evaluated to determine the one that better adjust to the goals of this project.

Horseshoe Canyon formation presents several coalbeds that can be separated in three coal zones. There are Carbon Thompson, Daly-Weaver and Drumheller Coal Zone. In general, Horseshoe Canyon coals are discontinuous and the seams thickness varies between 1-2m (Beaton et al., 2002). In addition, some Horseshoe Canyon coalbeds produce freshwater and in some areas they have become protected zones due to the important water source that they represent (Beaton A., 2003). In the case of the Bashaw Field, the well logs available show thin coal seams (1.5-2m) between 300 and 400m.

Mannville Group coal zones are deeper than Horseshoe Canyon coal zones. The average net coal thickness is 2-6m and it has been estimated high content of methane (Beaton A., 2003). In the Red Deer area, the Mannville coals can reach a net thickness in the range of 6-12m (Beaton A., 2003). Another factor to consider is that the Mannville coals are wet and the salinity of the water is generally high (Finn et al., 2009). In the Corbett Creek area, well logs reveal the Mannville coals at a depth of approximately 980m. Two coal seams can be easily identified: the Main seam of 3.65m and a Lower seam with a thickness of 1.67m.

The Mannville coals data set in the Corbett Creek area was selected for this project, based on the presence of thicker coalbeds that can storage bigger quantities of CO_2 and that can generate a bigger effect in the seismic response that will be evaluated in this study. Another factor taken into account during the selection of the data set was that Mannville coals are deeper and produce saline water avoiding the risk of affecting protected zones that represent a source of freshwater by CBM production and CO_2 injection.

Once the Corbett field dataset was selected, data of physical properties of the Mannville coals were collected from previous studies.

Fluid Simulation

A fluid simulation was done with F.A.S.T CBM software, using data of the well 100-03-22-062-06W500. In this case, it was considered that the coal seam is a homogeneous media and a tank model (For example FIG. 6) was used to perform the simulation. A tank model implies that between two points there is no change in the reservoir properties and that an average of the properties can provide a good description of the reservoir (Odeh, 1969). Figure 6 presents a diagram of the tank model.

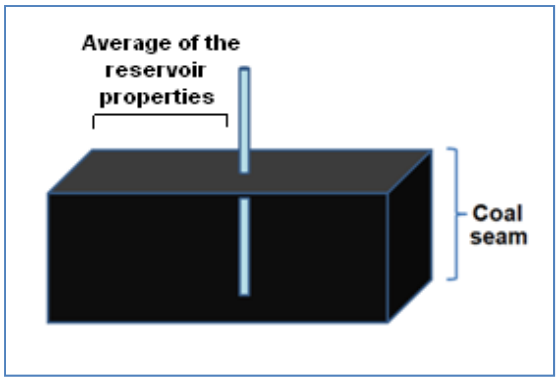

FIG. 6. Tank model assumed for fluid simulation. This model establishes that the properties of the reservoir do not vary from point to point, instead and average of the properties is used.

The parameters used to describe the coal seam for the fluid simulation are presented in Table 1.

Table 1. Reservoir and pore fluid parameters

Parameter	**Value**	**Source**
Reservoir Temperature	40°C	Accumap
Initial Reservoir Pressure	9140 KPa	Accumap
Permeability	3mD	Gentzis et al., 2008
Porosity	0.2%	Marvor et al., 2004
Net Thickness	5m	Well log data. Accumap
Coal density	1.3 g/cc	Gentzis and Bolen, 2008
Area	0.323 Km^2	F.A.S.T CBM Default
Wellbore skin value	-2	Gentzis and Bolen, 2008
Water Salinity	60000 ppm	Finn et al., 2009
Methane Gravity	0.56	Batzle and Wang, 1992
Initial water saturation	100%	-----
Initial Gas composition	100% CH_4	-----

The fluid simulation can be divided in three stages: construction of the Langmuir Isotherm, modeling of the matrix shrinkage and deliverability and production forecast.

Construction of the Langmuir Isotherm

In this stage of the simulation, the Langmuir parameters as well as the initial reservoir properties are necessary to built desorption Isotherm. Table 2 shows the methane Langmuir parameters.

Table 2. Methane Langmuir Parameters

Parameter	**Value**	
Langmuir Methane Volume	11.76 cm^3/g	Marvor and Gunter, 2006
Langmuir Methane Pressure	4688.43 KPa	Marvor and Gunter, 2006

The desorption isotherm obtained with the parameters in Table is presented in FIG. 7.

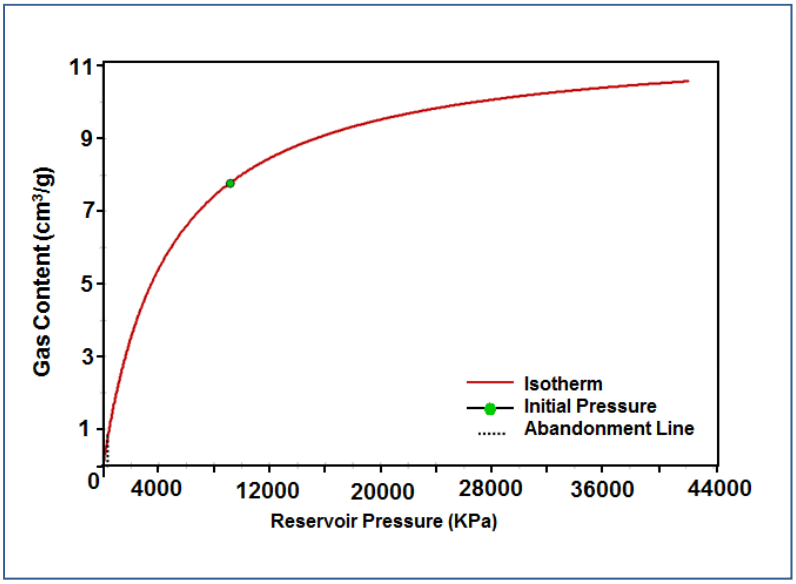

FIG. 7. Desorption Isotherm. This curve determines the methane desorpted from the coal matrix at an specific reservoir pressure.

Matrix Shrinkage/Swelling

Changes in the porosity and permeability due to swelling and shrinkage of the matrix where calculated using the Palmer and Mansoori analytical model (Palmer and Mansoori, 1998). The parameters required to complete this stage are presented in the Table 3.

Table 3. Parameters for Palmer and Mansoori model.

Parameter	**Value**	
Poisson Ratio	0.21	Marvor and Gunter, 2006
Young modulus	2435.0MPa	Marvor and Gunter, 2006
Bulk Modulus	1399.5MPa	Marvor and Gunter, 2006

Palmer and Mansoori model (Palmer and Mansoori, 1998) provide information about the variation of the porosity ratio (final porosity divided by initial porosity) with pressure.

Deliverability and production forecast

In this stage, the relative permeability curves were included in the model. For this project, it was not possible to find relative permeability curves for the area of study. In 2008, Gentzis and Bolen use the relative permeability curves of Maney and Paterson (1996) for Australian coals, to do a fluid simulation for the Gates coals, the Mannville coals equivalent in the Alberta´s Foothills. This curve was also used for the development of this project. The relative permeability curves are shown in FIG. 8.

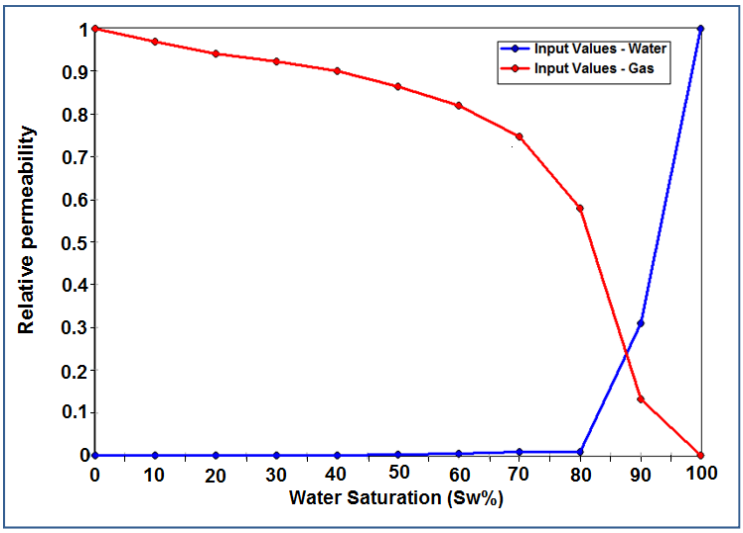

FIG. 8. Relative Permeability curves.

The production forecast provided an estimation of the reservoir behaviour during the first 10 years of production and it was calculated based on desorption isotherms, the Palmer and Mansoori model (Palmer and Mansoori, 1998) and the relative permeability curves.

Shear wave velocity estimation

The estimation of the velocity of the shear wave was done with the empirical relation of Marcote-Rios. This empirical relation is the result of laboratory tests conducted on Australian coal samples of different ranks. Equation 6 presents the Marcote-Rios relation,

$$V_s = 0.4811\, V_p + 0.00382 \ , \qquad (6)$$

with the velocity in Km/s. (Mavko et al, 2009)

Gassmann fluid substitution

Fluid substitution was performed following the steps provided by Smith et al. (2003) and Kumar (2006) in their tutorials for the application of the Gassmann equation (Gassmann, 1951). The fluid substitution process can be divided in two phases: the determination of the in-situ properties as well as the physic rock properties and the estimation of the properties assuming a new fluid mix in the pore space.

For the phase I of the process, we use the sonic and density logs of the well 100-03-22-062-06W500 (FIG. 5) to determine the in-situ properties. For the initial condition, it was assumed that the pore fluid is 100% brine. The bulk modulus of the saturated rock, at in-situ conditions, was calculated using the following equation:

$$K = \rho_b \left(V_p^2 - \frac{4}{3} V_s^2\right) , \quad (7)$$

where ρ_b corresponds to the bulk density taken from the density log, V_p is the velocity of the compressional wave obtained from the sonic log and V_s is the estimated shear wave velocity (Kumar, 2006). Shear modulus G, which will be constant during the fluid substitution process is calculated according to: (Smith et al., 2003).

$$G = \rho_b V_s^2, \quad (8)$$

For the bulk modulus of the mineral matrix K_0, in this case we consider a monomineralic matrix composed of carbon.

The pore fluids properties were calculated using the CREWES Fluid Properties Explorer application (CREWES.org) (FIG. 9). The properties of the CH_4 were estimated with the equations of Batzle and Wang (1992) based on the methane specific gravity. Brine bulk modulus and density were also calculated with Batzle and Wang equations. To calculate the pore fluid properties, the reservoir pressure, reservoir temperature, water salinity and methane specific gravity where required. Table 4 presents the calculated Fluid Properties.

Table 4. Fluid properties at reservoir conditions.

Fluid property	**Value**
Liquid Phase:	
Brine Density	1.034 g/cm^3
Brine Bulk Modulus	2658.68 MPa
Gas Phase:	
Methane density	0.022 g/cm^3
Methane Bulk Modulus	5.397 MPa

In addition, it is necessary to calculate the bulk modulus of the frame of the rock K^* (dry rock) according to: (Smith et al., 2003).

$$K^* = \frac{K_{sat}\left(\frac{\phi K_0}{K_{fl}} + 1 - \phi\right) - K_0}{\frac{\phi K_0}{K_{fl}} + \frac{K_{sat}}{K_0} - 1 - \phi} , \quad (9)$$

where K_{sat} is the bulk modulus of the saturated rock, K_0 is the bulk modulus of the mineral matrix, K_{fl} is the bulk modulus of the fluid in the pore space and ϕ is the fractional porosity (Smith et al., 2003).

The second phase of the fluid substitution begins with the estimation of the properties of the new fluid ρ_{flmix}. Based on the results of the fluid simulation, the new fluid properties were calculated for the well 100-03-22-062-06W500 after 8 years of production. At this time the fluid saturations are 82.1% of brine and 17.9% of CH_4. A

porosity update was also applied. The density of this mix of fluids is calculated according to:

$$\rho_{flmix} = \phi_{CH_4}\,\rho_{CH_4} + \phi_{brine}\,\rho_{brine} \quad , \tag{10}$$

where ρ_{CH_4} and ρ_{brine} are the methane and brine density respectively, and ϕ_{CH_4} and ϕ_{brine} are the volume fraction of each component (Batzel and Wang, 1992). The bulk modulus for this mix of fluids was calculated according to:

$$\frac{1}{K_{flnew}} = \frac{\phi_{CH_4}}{K_{CH_4}} + \frac{\phi_{brine}}{K_{brine}} \quad , \tag{11}$$

where K_{CH_4} and K_{brine} are the bulk modulus of the CH_4 and brine (Batzle and Wang, 1992) previously calculated with the CREWES Fluid Properties Explorer application (CREWES.org).

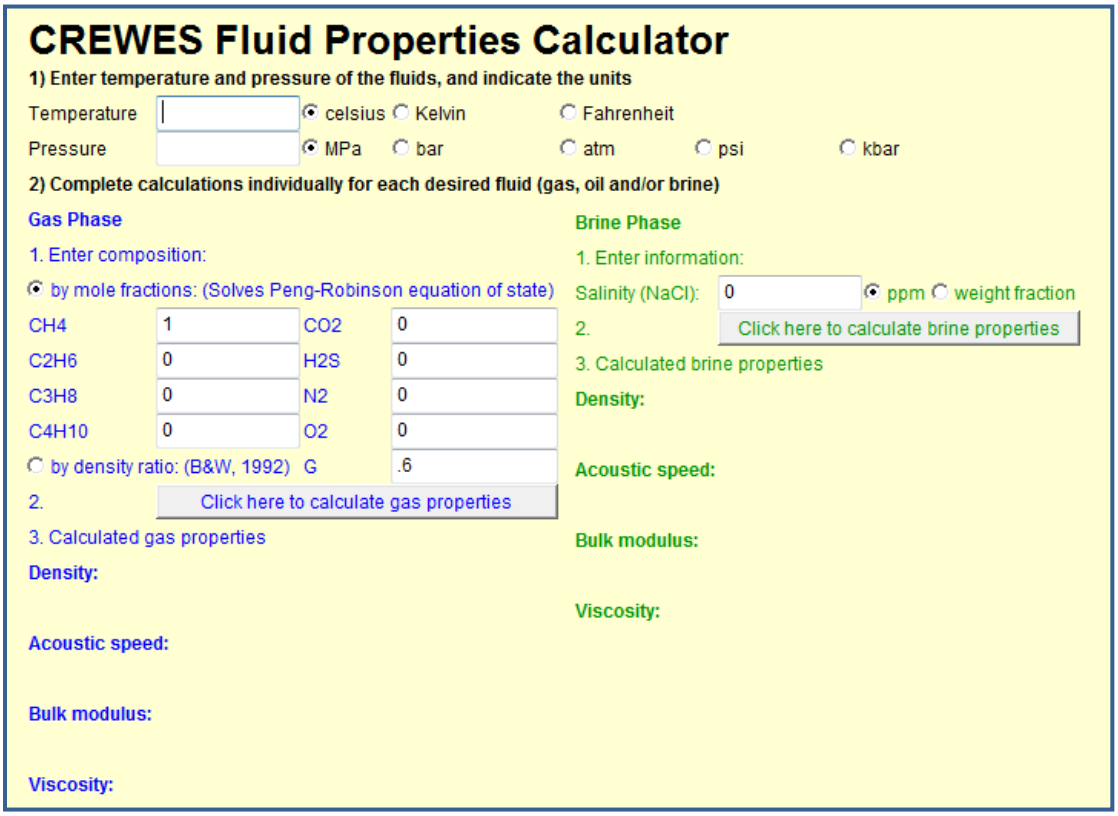

FIG: 9. CREWES Fluid Properties Explorer application (CREWES.org) for gas and brine phase.

Once the rock and fluid in-situ properties and the properties of the new mix of fluids are calculated, it is possible to determine the bulk modulus of the rock saturated with the new fluid using equation 5 (Smith et al., 2003).

The new bulk density of the rock, ρ_{bnew}, after the fluid substitution, is calculated according to:

$$\rho_{bnew} = \rho_g(1-\phi) + \rho_{flmix}\phi\,, \tag{12}$$

where ρ_g is the matrix density (Smith et al., 2003). Finally the velocity of the compressional and shear waves is estimated with equation 7 and 8 using the bulk modulus of the rock, saturated with the new fluid (Smith et al., 2003).

Synthetic Seismograms

The Synthetic seismograms were generated in time and depth domain, using the CREWES Software SYNGRAM (CREWES.org). In order to identify the effect of the replacement of brine by CH_4, synthetic seismograms before and after fluid substitution were generated.

Also, for this project, some tests were done to evaluate the seismic response in presence of coal seams of different thickness. For the first case we use the original data, with the Main seam of 3.65m and the Lower seam of 1.67m. The second case consists of a 10.64m coal seam while the third one is a 21.28m seam.

A 30 Hz and 60Hz zero phase Ricker wavelets (FIG. 10) were created using CREWES WAVELETED facility (CREWES.org). In terms of the receivers' geometry, the far offset parameter was set to 2000m and the receiver interval to 50m.

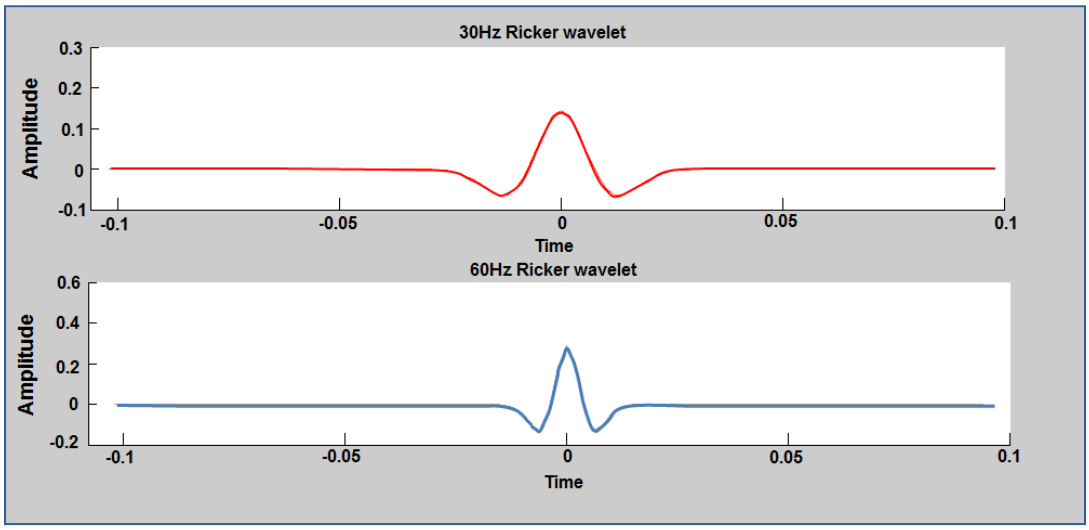

FIG. 10. 30Hz and 60Hz Ricker wavelets for synthetic seismograms.

RESULTS

Fluid Simulation

The fluid simulation performed with the F.A.S.T CBM software, provided information about the changes that occur in the coal matrix during methane production and an estimation of gas and water production rates in a 10 years period.

The changes in the coal matrix were estimated in terms of the porosity ratio $\frac{\phi}{\phi_i}$ where ϕ is the cleat porosity and ϕ_i is the cleat porosity at initial reservoir pressure using the Palmer and Mansoori Model.

Figure 11 presents the variation of the porosity ratio with the reservoir pressure. This graph shows a decrease in the porosity ratio as the reservoir pressure decrease from 9000KPa to 3500KPa. In the case of primary production, which is the case studied in this project, the behaviour of the curve (in this range of pressure) can be described as a consequence of effective stress augmentation. The change in the effective stress occur when reservoir pressure decrease during depletion while the stress due to the overburden remains constant (Shi and Durucan, 2005). This leads to a decrease in the permeability/porosity as a result of the compression suffered by cleats which is evident in this section of the curve.

At pressures lower than 3500KPa there is a change in the curve's behaviour (FIG. 11), showing an increment of the porosity ratio. The decrease of the reservoirs pressure due to depletion also causes methane's desorption and as a consequence the shrinkage of the coal matrix. This process represents an increase in the permeability/porosity (Palmer and Mansoori, 1998). At pressure below 3500KPa the increase in the porosity occurs because at this point the effect on permeability/porosity of the shrinkage of the matrix overcomes the effect caused by the augmentation of the effective stress.

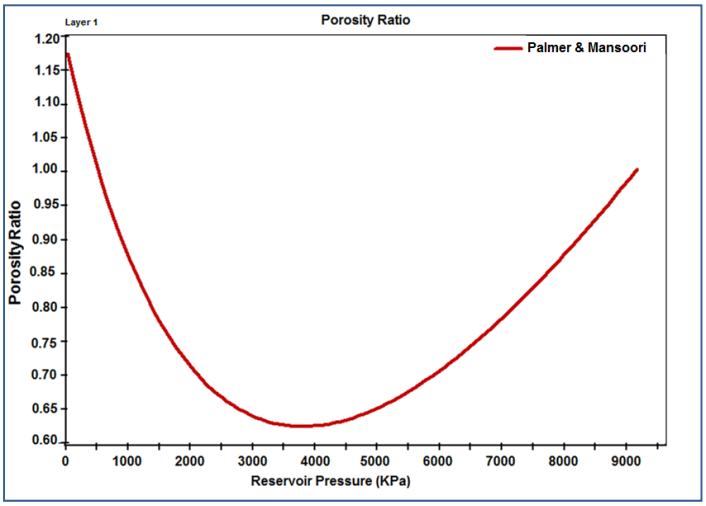

FIG. 11. Variation of the Porosity ration with the Reservoir pressure estimated with Palmer and Mansoori model (Palmer and Mansoori, 1998)

Figure 12 presents the gas and water production forecast. For the water rate forecast (blue line in FIG. 12) a rapid decrease in the water production rate is evident during 2010 and the beginning of 2011 which corresponds to the dewatering period. After this, the water production rate slowly decreases with the pass of the years. The gas production rate (red line in FIG. 12) rapidly increase until it reaches its maximum point at 7500m^3/d. Then, the gas production rate start to decrease until it stabilizes approximately 4 years after the first day of production.

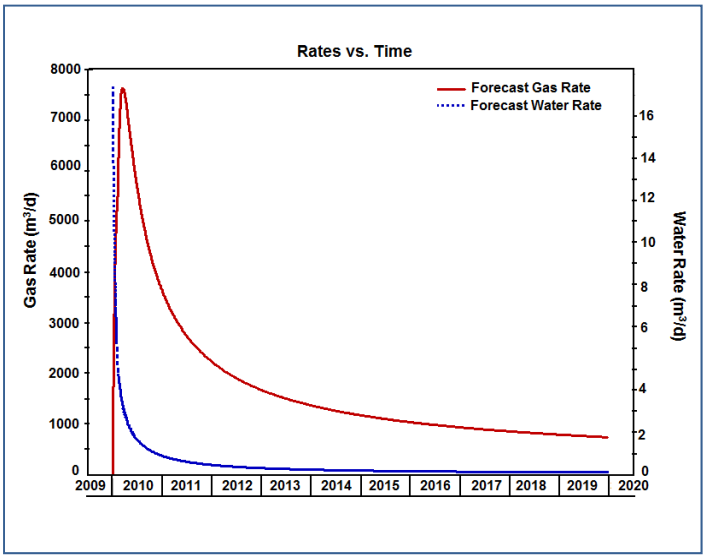

FIG. 12. Gas and Water production rates forecast. This graph provides an estimation of the gas and water production per day along a 10 years period, starting the first day of production.

In addition, Table 5 presents the variation of the water saturation during reservoir depletion along a 9 year period. This table present the progressive decrease of the water saturation and the increase of the presence of methane.

Table 5. Water Saturation variation with pressure

Date	Pressure (KPa)	Water Saturation %
01/01/2010	8931.01	90.85
01/01/2011	6457.335	85.096
01/01/2012	5526.985	84.114
01/01/2013	4964.689	83.511
01/01/2014	4563.482	83.084
01/01/2015	4251.019	82.756
01/01/2016	3995.132	82.495
01/01/2017	3777.956	82.278
01/01/2018	3590.289	82.096
01/01/2019	3424.807	81.939

The data obtained from the fluid simulation allowed the estimation of the water and gas saturation after 8 years of production and also linked this information to a reservoir pressure and an updated porosity providing a complete scenario for fluid substitution.

Synthetic seismograms

The synthetic seismograms generated give an idea of the character of the seismic response of the coalbeds saturated with 100% brine and with 82.1% of brine and 17.9% of methane. Synthetic seismograms using different wavelets and different coal thicknesses are presented.

Case 1: Main seam 3.65m and Lower seam 1.67m

As it occurs in Corbett Field (FIG. 5), this case evaluates the seismic response of two coal seams: the Main seam of 3.65m and the Lower seam with a thickness of 1.67m. Figure 13, present the synthetic seismograms generated with a 30Hz zero phase Ricker wavelet. In Figure 13, the synthetic seismograms present a negative reflection at a depth of approximately 980m. This trough corresponds to the top of the Main seam as it can be correlated with the logs. At a depth of approximately 1000m it is possible to appreciate a positive reflection. In this case, this peak can be associated with the response of a thin coal seam (below the Lower seam) located at around 1000m. In this case, the Main Seam, the Lower seam and the coal seam at a depth of 1000m are being resolved as a complete unit or block.

Figure 13a represents the synthetic seismogram for the coalbeds saturated with 100% brine. The reflections associated to the top and base of the three coalbeds are weak and there is no evident AVO response. Figure 13b presents the seismogram for the coalbeds saturated with 82.1% brine and 17.9% methane. After the fluid substitution, it is possible to appreciate an increase in the amplitude of the reflections mentioned before, caused by the decrease in the P-wave velocity after substituting brine by CH_4.

Comparing the well logs in Figure 13a and 13b, there is an important diminution of the P wave velocity. The average velocity for the coalbeds saturated with 100% brine is 2370m/s and after substituting the brine by methane the average P-wave velocity is 1670m/s. The density log also presents a small diminution after fluid substitution. In the case of the S-wave velocity, a moderate velocity increase occurs as it was expected.

Figure 14 shows the synthetic seismograms generated with a 60Hz zero phase Ricker wavelet. The obtained results are similar to the ones generated with the 30Hz Ricker but in this case the amplitude variation becomes more evident. With the 60Hz Ricker wavelet is still not possible to resolve the Main and Lower seam.

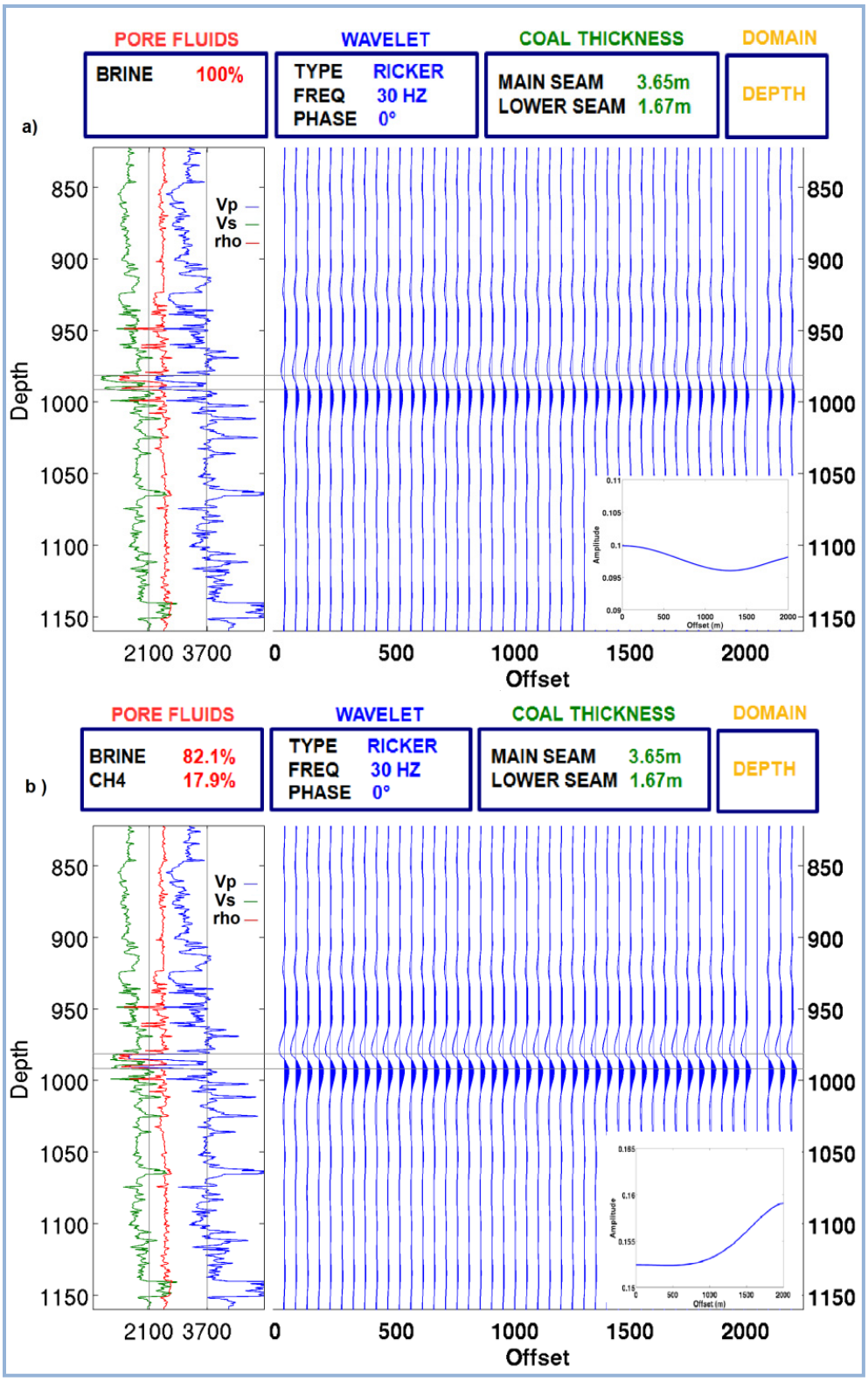

FIG. 13. Synthetic seismograms for two coal seams (Main and Lower seam), generated with a 30Hz zero phase Ricker wavelet. a) coalbeds are saturated with 100% brine, b) coalbeds are saturated with 82.1% brine and 17.9% methane.

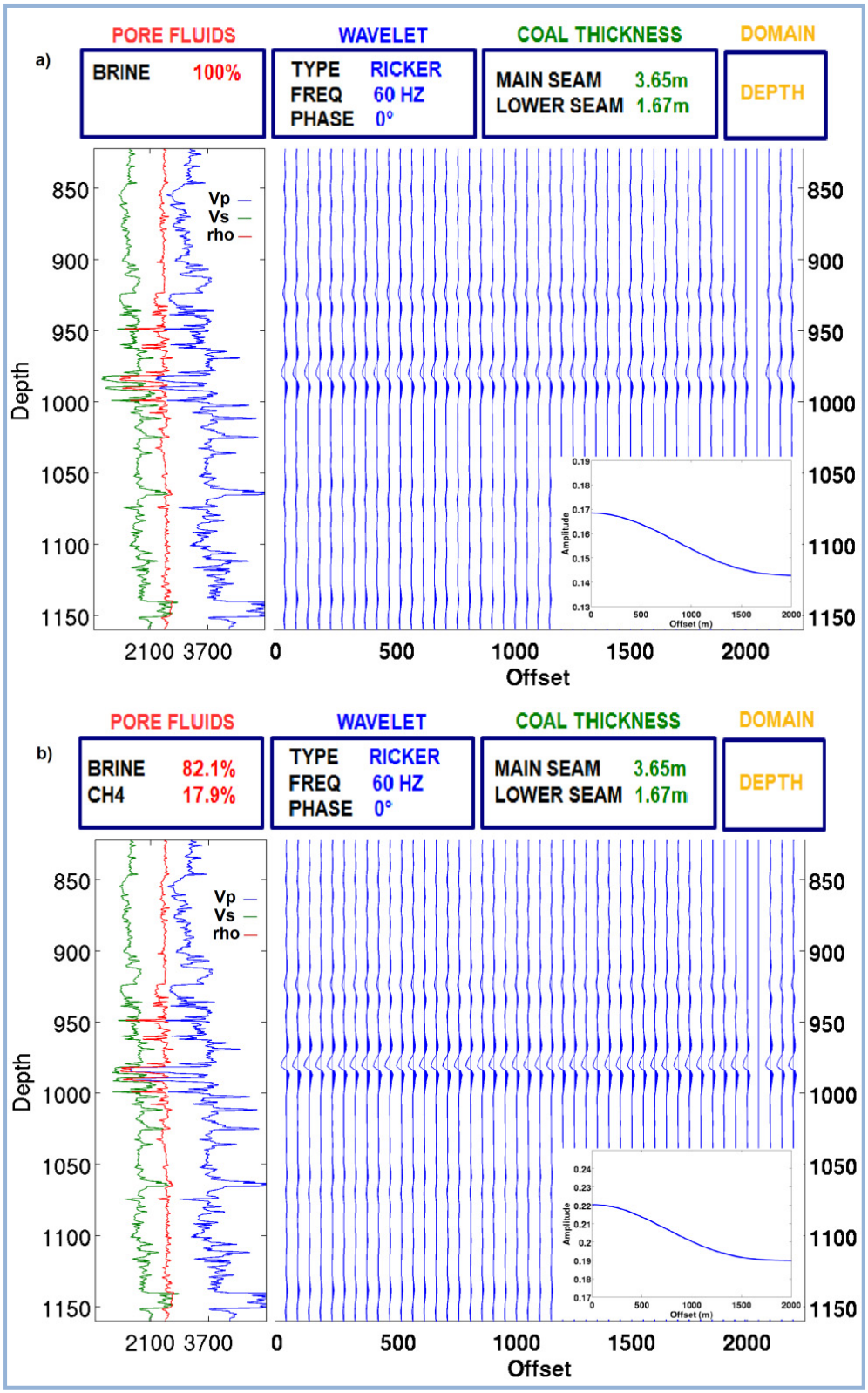

FIG. 14. Synthetic seismograms for two coal seams (Main and Lower seam), generated with a 60Hz zero phase Ricker wavelet. a) coalbeds are saturated with 100% brine, b) coalbeds are saturated with 82.1% brine and 17.9% methane.

Case 2: Coal seam with a thickness of 10.64

In this case, the well log data corresponding to the Main Seam and the Lower seam were put together and duplicated to create a coal seam of 10.64m thickness.

The synthetic seismograms in Figure 15 were generated with a 30Hz Ricker wavelet. The amplitude trough at a depth of 980m coincides with the top of the coalbed while the peak at around 990m can be associated with the base of the coalbed. In this case the reflections seem to be stronger compared with their equivalents in Case 1. In addition, there is still no evidence of variation of the amplitude in function of the offset.

In synthetic seismograms in Figure 15a the fluid present in the coalbed is 100% brine and the top and the base of the coalbed can be easily identified as the strongest reflections in the seismograms. Figure 15b shows the synthetic seismograms for the coalbed saturated brine and methane. The replacement of brine by methane using Gassmann fluid substitution (Gassmann, 1951) caused a change in the character of the wavelet, presenting an amplitude increasing and a phase shift.

The synthetic seismograms generated with the 60Hz Ricker wavelet are presented in Figure 16 in the time domain and in Figure 17 in the depth domain. The idea of presenting the seismograms in both domains is to evaluate the existence of advantages that one domain can offer over the other.

For the coal seam saturated with brine (FIG. 16a), in the time domain, there is a trough at approximately 0.65s that correlates with the top of the coalbed and a peak at approximately 0.66s that represents the base of the coalbed. Furthermore, now it is possible to appreciate a small decrease of the amplitude for larger offset. When the coalbed is saturated with water and methane (FIG. 16b), the synthetic seismograms present a time delay showing the bottom of the coalbed at approximately 0.67s. The fluid substitution also produces an increase in the amplitude and a phase shift.

In the depth domain (FIG. 17) the reflections associated with the top and base of the coal seam are at a depth of 980m and 990m respectively and an AVO response is observed as a decrease of the amplitude with the offset. The variations in character of the wavelet are also evident in this domain after fluid substitution. Comparing both domains, the effect of the presence of methane in the seismic response becomes more evident in the depth domain than in time, making easier the determination of the changes that are consequence of the Gassmann fluid substitution (Gassmann, 1951).

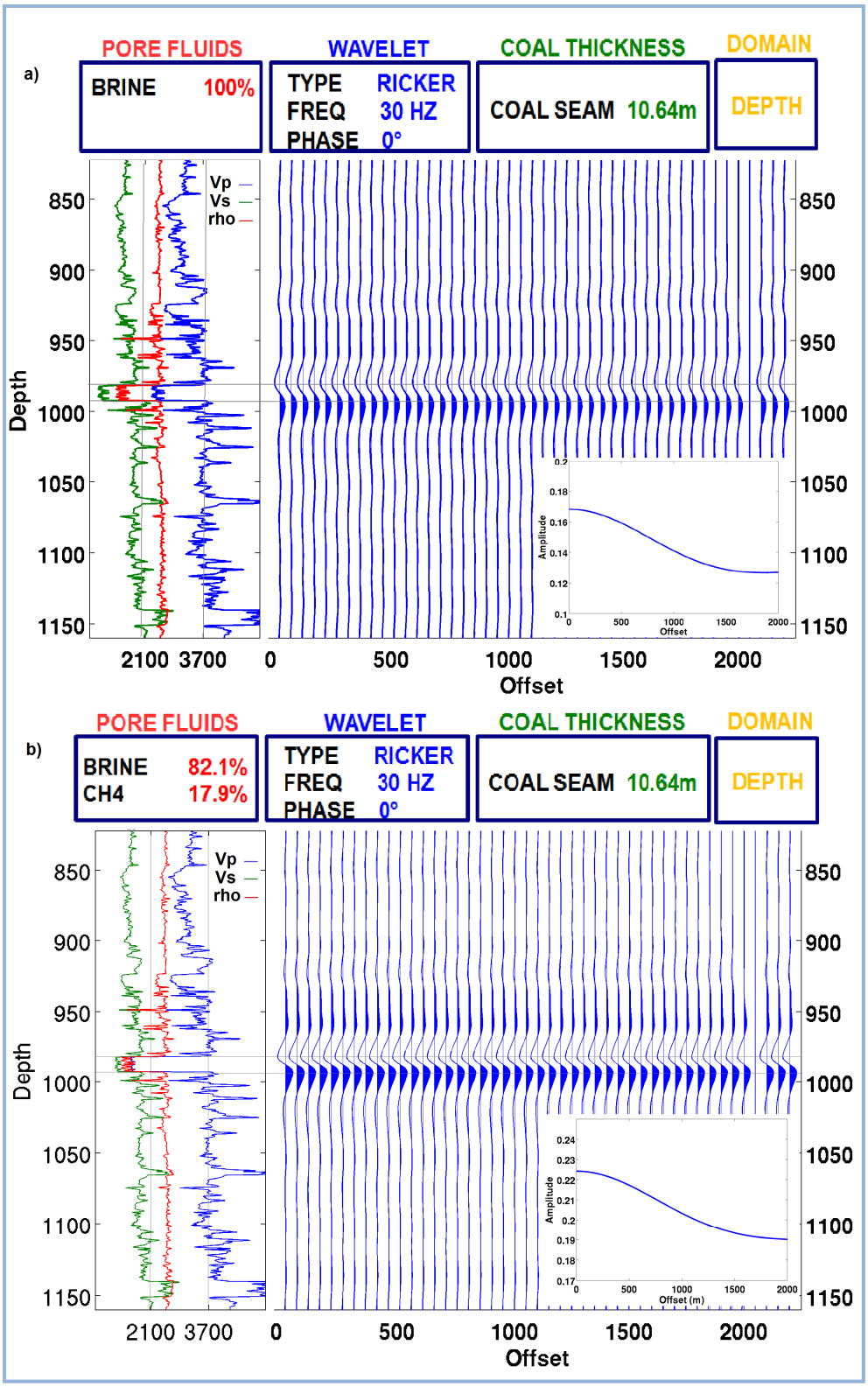

FIG. 15. Synthetic seismograms for a 10.61m coalbed, generated with a 30Hz zero phase Ricker wavelet. a) coalbeds are saturated with 100% brine, b) coalbeds are saturated with 82.1% brine and 17.9% methane.

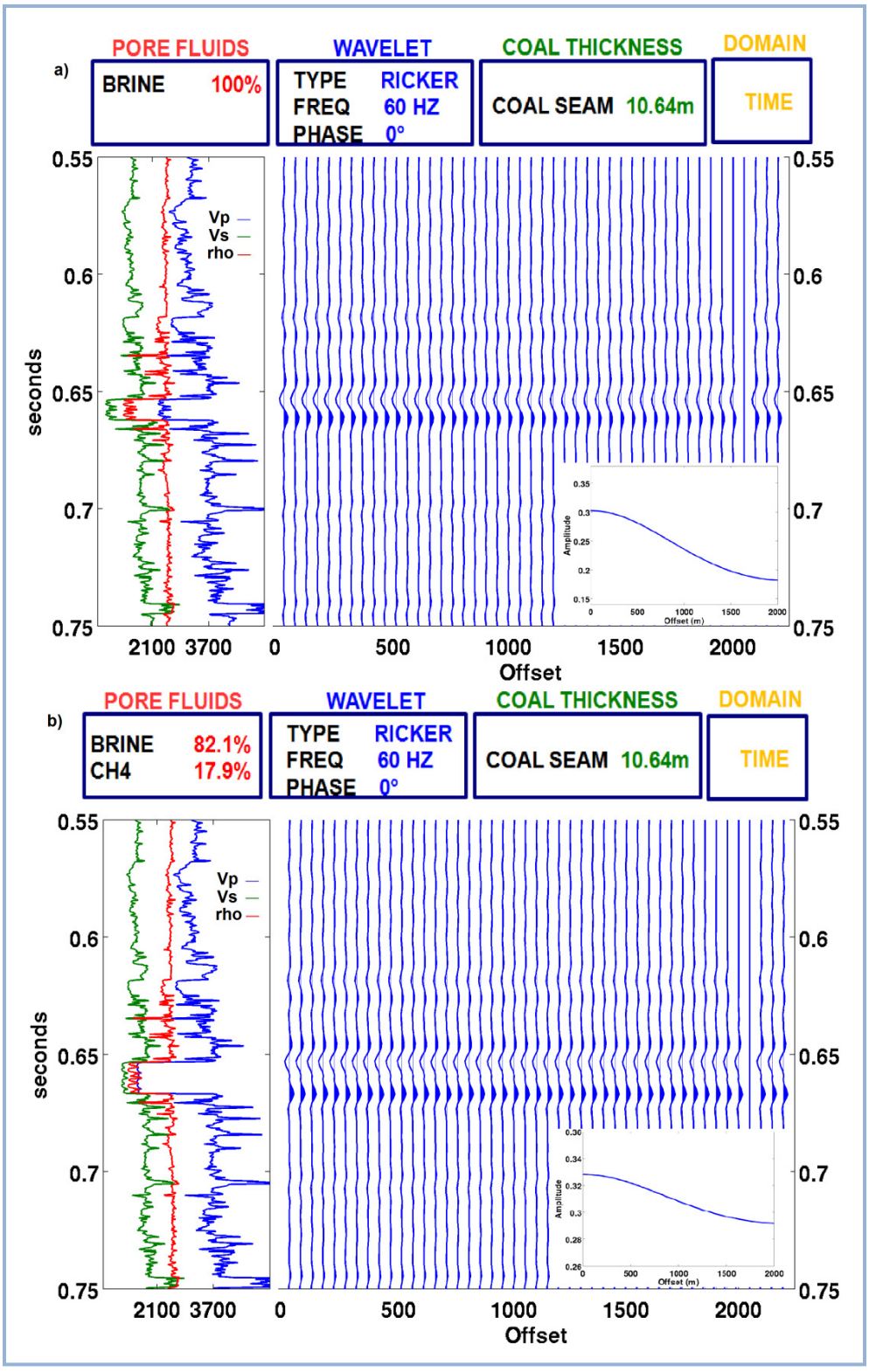

FIG. 16. Time domain synthetic seismograms for a 10.61m coalbed. Generated with a 60Hz zero phase Ricker wavelet. a) coalbeds are saturated with 100% brine, b) coalbeds are saturated with 82.1% brine and 17.9% methane.

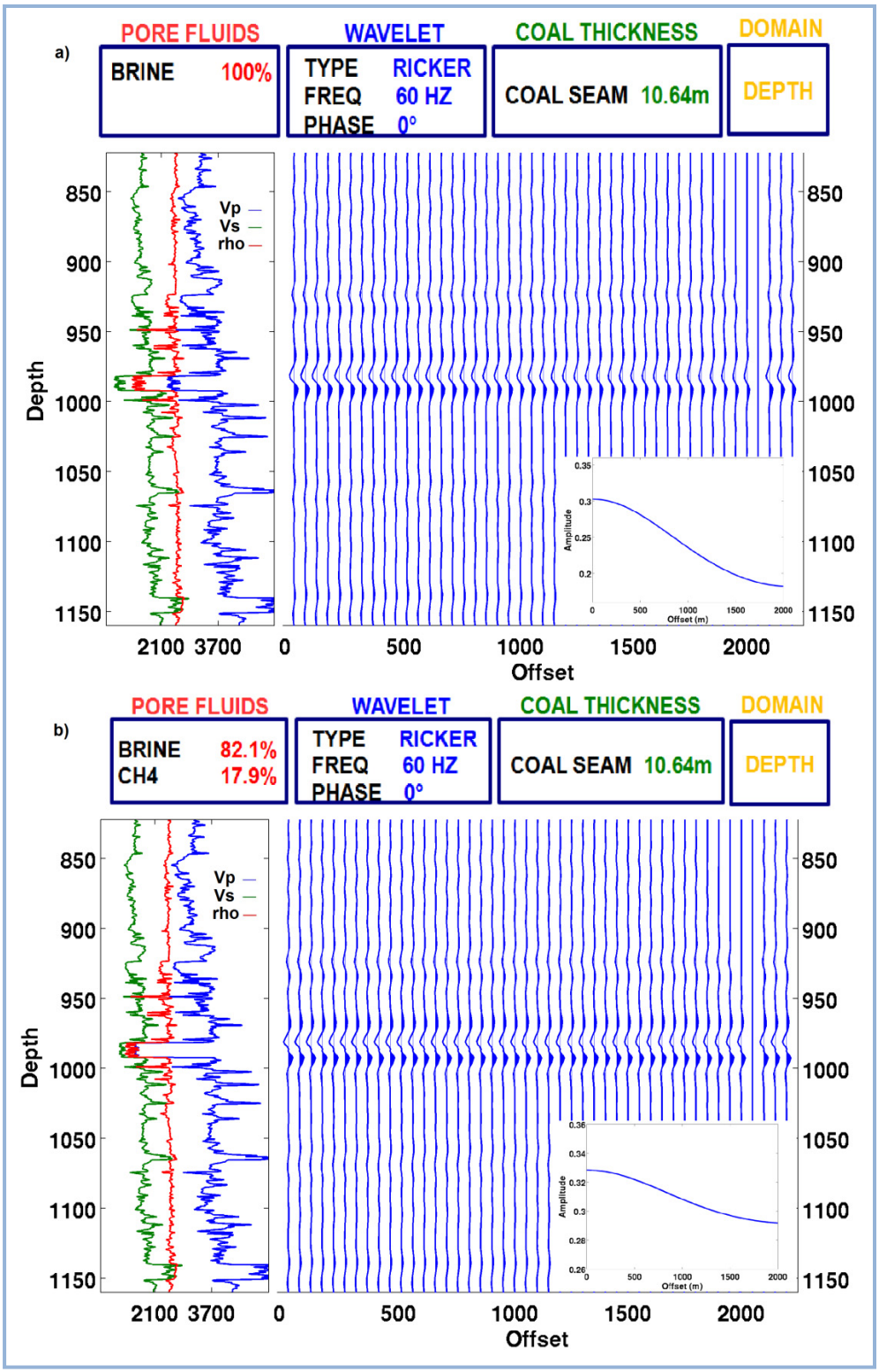

FIG. 17. Depth domain synthetic seismograms for a 10.61m coalbed. Generated with a 60Hz zero phase Ricker wavelet. a) coalbeds are saturated with 100% brine, b) coalbeds are saturated with 82.1% brine and 17.9% methane.

Case 3: Coal seam with a thickness of 21.28

In this case, the data of the coalbed in the case 2 was duplicated to form a coalbed with a thickness of 21.28m.

Figure 18 is the time domain synthetic seismograms for a 21.28m coalbed and it was generated with a 30Hz zero phase Ricker wavelet. When the fluid present in the pore space is 100% brine (FIG. 18a) the reflections that correspond to the top and base of the coalbed are strong at around 0.65s and 0.67s respectively. These reflections have bigger amplitude compared with their equivalent in Case 1 and Case 2. Also, there is an AVO response with amplitude decreasing with offset. For a brine and methane saturated coal seam (FIG. 18b), there is a time delay in the reflection associated with the base of the coalbed, which appears at around 0.68s. After fluid substitution, the character of the wavelet completely change presenting a lightly increase of the amplitude of the reflections and a shift in the phase. The AVO response becomes less obvious after substituting brine by methane.

The depth domain synthetic seismogram for the 21.28m coal seam that was generated with a 30Hz Ricker wavelet is displayed in Figure 19. Before fluid substitution (FIG. 19a), at approximately 980m appears the reflection of the top of the coalbed while the one related to the base is close to a depth of 1000m. A decrease of the amplitude with the offset is also observed in the depth domain. With 82.1% of brine and 17.9% of methane in the pore space (FIG. 19b), the changes in the character of the wavelet follow the pattern observed in the time domain. Comparing the synthetic seismograms in time and depth domain (FIG. 18 and 19), the depth domain provides the opportunity of a direct evaluation of the variations that occur as a consequence of the fluid substitution avoiding the time shift present in the time domain seismograms.

Finally, Figure 20 shows the synthetic seismograms generated with a 60Hz zero phase Ricker wavelet. In these synthetic seismograms, the coalbed is clearly resolved and defined by strong reflections associated with the top and base. In this case, an AVO response is not observed. Between the top and the base reflection of the coalbed, there is a positive reflection or peak, which is the one that is providing the information of the fluids in the pore space. In Figure 20a, this reflection has small amplitude while In Figure 20b, this reflection show an increase of the amplitude due to the effect of the fluid substitution.

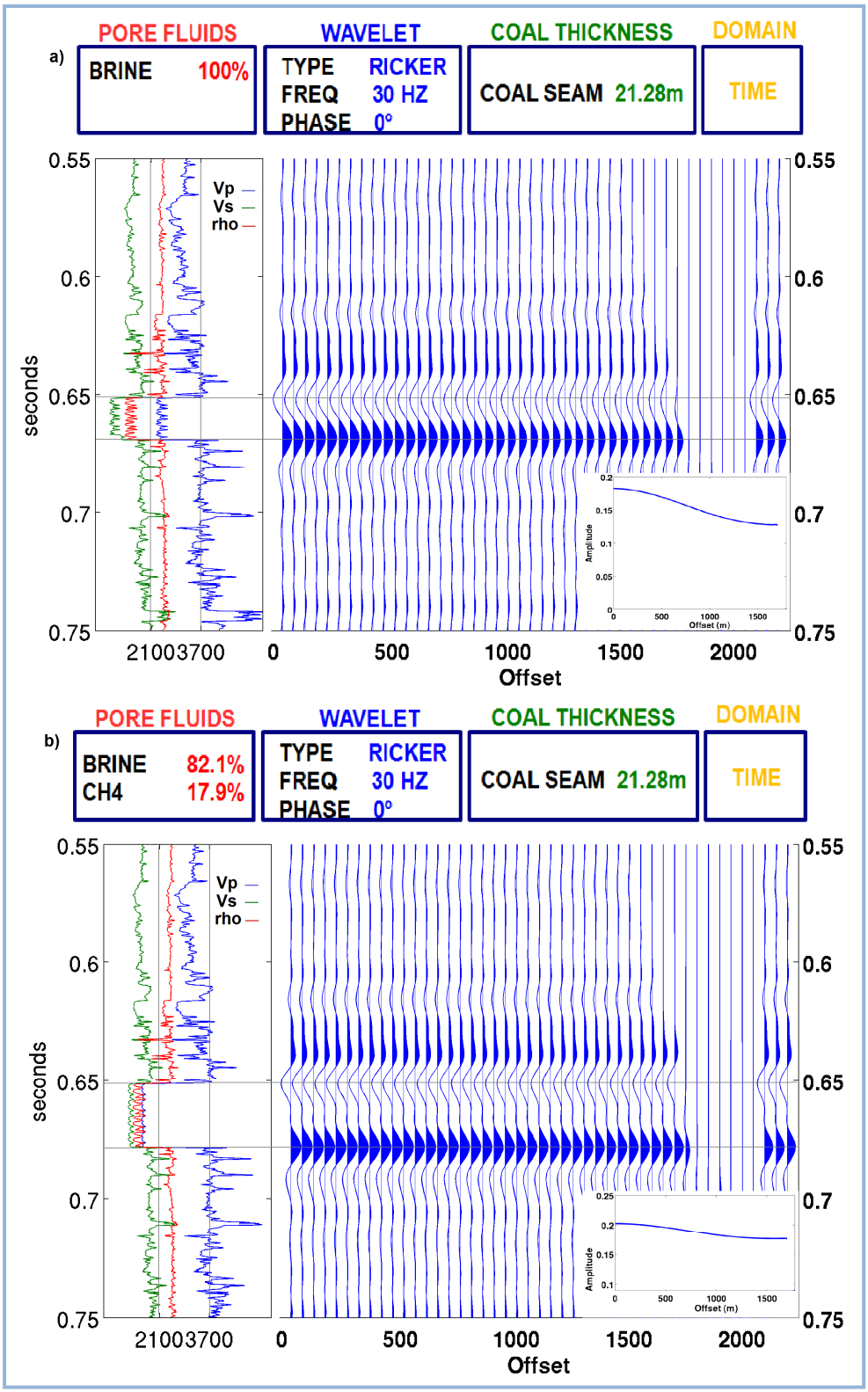

FIG. 18. Time domain synthetic seismograms for a 21.28m coalbed, generated with a 30Hz zero phase Ricker wavelet. a) coalbeds are saturated with 100% brine, b) coalbeds are saturated with 82.1% brine and 17.9% methane.

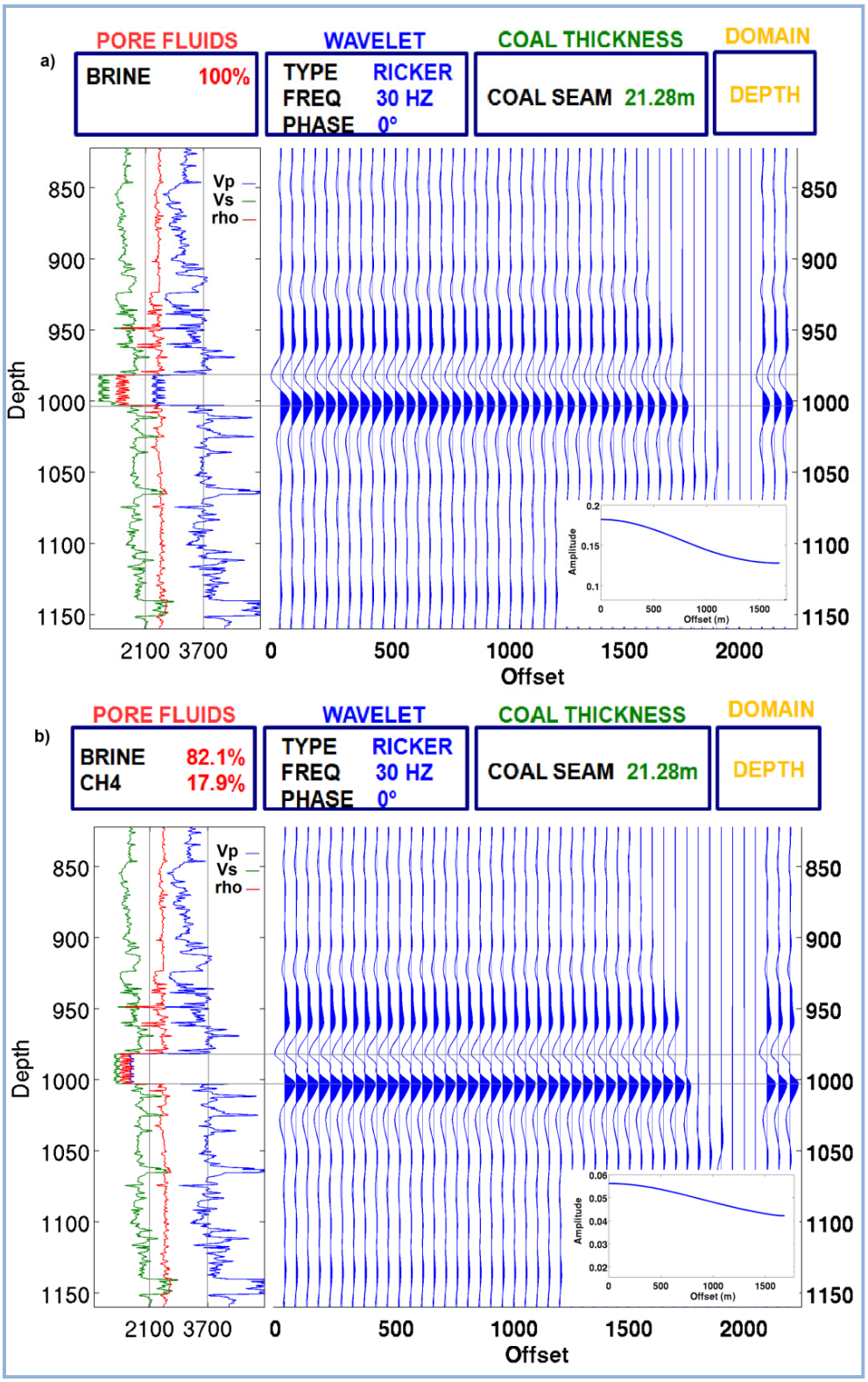

FIG. 19. Depth domain synthetic seismograms for a 21.28m coalbed, generated with a 30Hz zero phase Ricker wavelet. a) coalbeds are saturated with 100% brine, b) coalbeds are saturated with 82.1% brine and 17.9% methane.

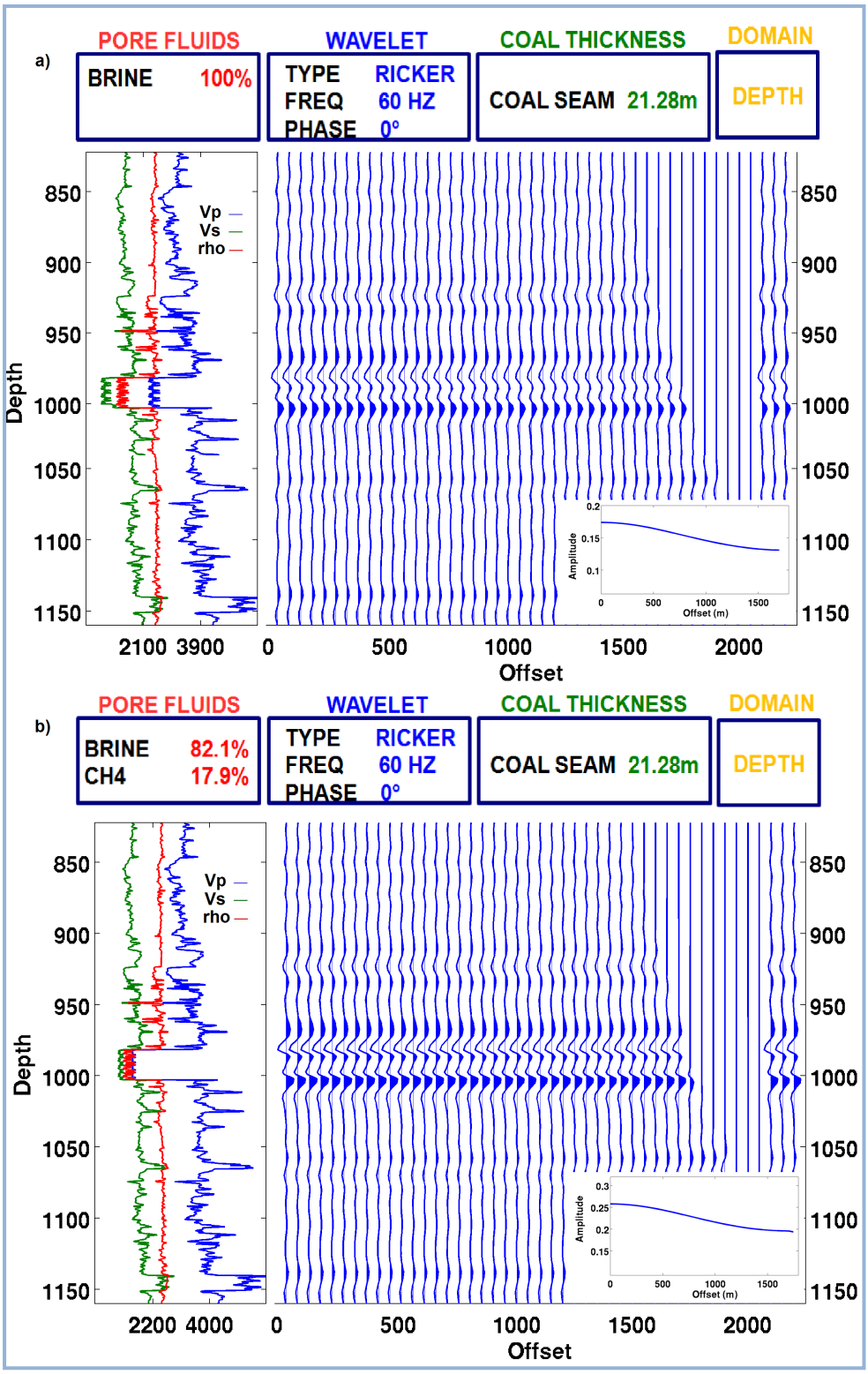

FIG. 20. Synthetic seismograms for a 21.28m coalbed, generated with a 60Hz zero phase Ricker wavelet. a) coalbeds are saturated with 100% brine, b) coalbeds are saturated with 82.1% brine and 17.9% methane.

CREWES Zoeppritz Explorer

The CREWES Zoeppritz (CREWES.org) explorer was use to evaluate the variations of the reflection coefficients with the incidence angle.

For the use of this interface and average of the P-wave velocity, S-wave velocity and density of the layer that overlays the coalbed was calculate and use as the upper layer parameters. For the upper layer the P-wave velocity is 3162m/s, the S-wave velocity 1525m/s and a density of 2432Kg/m^3. The coalbed parameters were introduce as the lower layer parameters. The parameter used were the P-wave velocity is 2377m/s, the S-wave velocity 873m/s and a density of 1436Kg/m^3

The evaluation of the Zoeppritz equation using the data mentioned before is presented in Figure 21. From this graph, it can be interpreted that there is not a critical angle over which the reflection coefficient becomes or approximates to zero. For incidence angles between 0° and 55° the amplitude will tend to slowly decrease and for incidence angles over that range the amplitude will have a representative increase.

Another important observation is that the reflection coefficients have a negative range indicating that in this case the top of the coalbed will be a always a trough which coincides with the observation in synthetic seismograms generated.

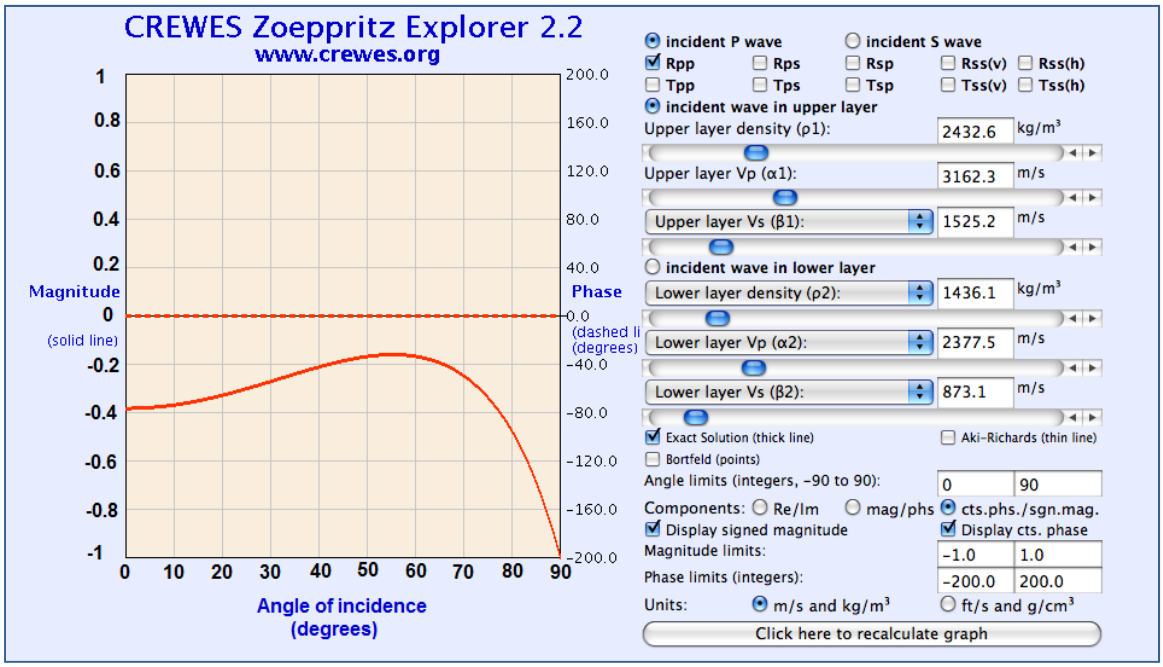

FIG. 21. CREWES Zoeppritz explorer (CREWES.org). Upper layer corresponds to an average of the overburden parameters and the lower layer is the coalbed

CONCLUSIONS

The evaluation of the synthetic seismograms generated with 30Hz and 60Hz Ricker wavelets, for different coalbed thicknesses gives an idea of the changes that we can expect depending on the fluid in the pore space of the coalbed.

In the Case 1, we evaluate two coal seams that is the real situation in the Corbett Creek area. In this case, using 60Hz Ricker wavelet, the seismic resolution is not enough to resolve the two seams separately and we only evidence a small change in amplitude after fluid substitution. In the second case, 10.64m coalbed, we identify the top and the base of the coal seam with the 30Hz Ricker wavelet and the 60Hz Ricker wavelet and also a change in the character of the wavelet. For a 21.28m coalbed the coal seam was resolved and accentuated changes in amplitude and phase occur after fluid substitution.

In this study it was necessary at least a 10m coalbed to be able to resolve it and observe representative changes in the seismic response due to the replacement of brine by CH_4. In this study we adapt the work flow developed by Zarantonello et al. (2010)to evaluate variation seismic response of coalbeds due to fluids, using well log data from the Corbett Field. Some adjustments in the selection of the initial parameters, like the mineral matrix bulk modulus, can improve the quality of the results. For future work it was suggested to try to build the Reuss and Voight bounds with coal data available in order to select a more precise value for the mineral matrix bulk modulus (Gary Mavko , personal conversation).

ACKNOWLEDGEMENTS

I would like to thank Chris Clarkson, Larry Lines, Gary Margrave, and Don Lawton for their advice during the development of the project. Mahdi Al-Mutlaq and Faranak Mahmoudian for their constant support. Gary Mavko for his comments and advices. Finally I would like to thank CREWES sponsors, staff and students.

REFERENCES

Bachu S. 2007. Carbon dioxide storage capacity in uneconomic coal beds in Alberta, Canada. Methodology, potential and site identification. International Journal of Greenhouse gas control I, 374-385.

Balan H. and Gumrah F. 2008. Enhanced Coalbed Methane Recovery with respect to physical properties of coal and operational parameters. Journal of Canadian Petroleum Technology 48, 56-61.

Banerjee I. and Goodarzi J. 1990. Paleoenvironmental and sulphur-boron contents of the Mannville (Lower Cretaceous) coals of the southern Alberta, Canada. Sedimentary Geology 67, 297-310.

Batzle M. and Wang Z. 1992. Seismic properties of pore fluids. Geophysics 57, 1396-1408.

Beaton et al. 2002. Coalbed Methane Potential of Upper Cretaceous-Tertiary strata, Alberta Plains. Alberta Geological Survey. EUB/AGS Earth Science Report 2002-06.

Beaton A. 2003. Production Potential of Coalbed Methane Resources in Alberta. Alberta Geological Survey. EUB/AGS Earth Science Report 2003-03.

Beaton A., Langenberg W. and Pana C. 2006. Coalbed methane resources and reservoir characteristics from the Alberta Plains, Canada. International Journal of Coal Geology 65, 93-113.

Bell G. and Rakop K. 1986. Hysteresis of methane/coal sorption isotherms. SPE15454.

Chen Z. et al. 2009. Investigation of CO_2 Injection Induced Coal-Gas Interactions. American Rock Mechanics Association. 43rd Symposium ARMA 09-099.

Clarkson C. and Bustin R. 2010. Coalbed Methane: Current Evaluation Methods, Future Technical Challenges. SPE 131791-MS

Clarkson C. et al. 2010. Predicting sorption-induced strain and permeability increase with depletion for coalbed methane reservoirs. SPE Journal 15, 152-159.

Cockbill J.R., Finn C.M. And Krawiec M.B. 2008. Economics of Mannville CBM Development: Drilling & Production Innovation at Corbett Creek. Canadian International Petroleum Conference Paper 2008-200.

Deisman N., Ivars D., Darcel C. And Chalaturnyk R. 2009. Empirical and numerical approaches for geomechanical characterization of coal seam reservoirs. International Journal of Coal Geology 82, 204-212.

Dvorkin J., Mavko G. and Gurevich B. 2007. Fluid substitution in shaley sediment using effective porosity. Geophysics 72, 1-8.

Finn C. et al. 2010. Maximum reservoir contact wells for coalbed methane exploitation: Corbett Creek case study. Annual AAPG Convention Abstracts 19, 49.

Gasperikova E. and Hoversten G.M. 2008. Gravity monitoring of CO_2 movement during sequestration: Model studies. Geophysics 73, WA105-WA112.

Gassmann, F. 1951. Über die elastizität poröser medien: Vierteljahrss-chrift der Naturforschenden Gesellschaft in Zurich 96, 1-23. Paper translation at http://sepwww.stanford.edu/sep/berryman/PS/gassmann.pdf.

Gentzis T. and Bolen D. 2008. The use of numerical simulation in predicting coalbed methane producibility from Gates coals, Alberta Inner Foothills, Canada: Comparison with Mannville coal CBM production in the Alberta Syncline. International Journal of Coal Geology 74, 215-236.

Gentiz et al. 2008. Coalbed methane producibility from the Mannville coals in Alberta, Canada: A comparison of two areas. International Journal of Coal Geology 74, 237-249.

Groenenberg H. et al. 2008. Guidelines for licensing CO_2 storage operation around the globe. The Leading Edge 27, 496-501.

Gunter B. CO_2 sequestration in deep “unmineable”coals seams. Presentation from Alberta Research Council.

Han D. and Batzle M. 2004. Gassmann’s equation and fluid-saturation effects on seismic velocities. Geophysics 69, 398-405.

Karacan C. 2007. Swelling-induced volumetric strains internal to a stressed coal associated with CO_2 sorption. International Journal of Coal Geology 72, 209-220.

Koperna G.J. and Oudinot A.Y. 2009. CO_2-ECBM/Storage Activities at the San Juan Basin's Pump Canyon Site. SPE 124002.

Koperna G.J. and Riestenberg D. Carbon Dioxide Enhanced Coalbed Methane and Storage. SPE 126627.

Kumar D. 2006. A tutorial on Gassmann Fluid Substitution: Formulation, Algorithm and Matlab Code. Geohorizons 11, 4-12.

Marvor et al. 2004. Alberta multiwell Micro-Pilot Testing for CBM properties, enhanced methane recovery and CO_2 storage potential. SPE90256.

Marvor J. and Gunter W. 2006. Secondary porosity and permeability of coal vs. gas composition and pressure. SPE Reservoir Evaluation & Engineering 9, 114-125.

Mavko G., Mukerji T. and Dvorkin J. 2009. The rock physics handbook. Cambridge, Second Edition.

McCrank J. and Lawton D. 2009. Seismic characterization of a CO_2 flood in the Ardley coals, Alberta, Canada. The Leading Edge 28, 820-825.

Odeh A. 1969. Reservoir Simulation…What is it?. Journal of Petroleum technology 21, 1383-1388.

Palmer I. and Mansoori J. 1998.How Permeability Depends on Stress and Pore Pressure in Coalbeds: A New Model. SPE Reservoir Evaluation & Engineering 1, 539-544

Palmer I. 2009. Permeability changes in coal: Analytical modeling. International Journal of Coal Geology 77, 119–126

Peng S. et al. 2006. Factors facilitating or limiting the use of AVO for coal-bed methane. Geophysics 71, C49-C56.

Robertson E.P. 2008. Improvements in measuring sorption-induced strain and permeability. SPE 116259.

Shi J. and Durucan S. 2005. A model for changes in coalbed permeability during primary and enhanced methane recovery. SPE Reservoir Evaluation & Engineering 8, 291-299.

Smith T., Sondergeld C. and Rai C. 2003. Gassmann fluid substitution: A tutorial. Geophysics 68, 430-440.

White D. 2009. Monitoring CO_2 storage during EOR at the Weyburn-Midale Field. The Leading Edge 28, 838-842.

Zarantonello S., Bevc D. and Harris J. 2010.integrated reservoir, petrophysical, and seismic simulation of CO_2 storage in coal beds. The Leading Edge 29, 184-190.